Available online at www.sciencedirect.com

SciVerse ScienceDirect

Ceramics International 39 (2013) 2069–2076

CERAMICS INTERNATIONAL

www.elsevier.com/locate/ceramint

Crystallization mechanism and ac conductivity studies on strontium barium niobate glass–ceramics

Mengjie Wang[a], Yong Zhang[b,*], Xiaolin Liu[a], Xiangrong Wang[b]

[a]State Key Laboratory of Organic–Inorganic Composites, Beijing University of Chemical Technology, Beijing 100029, China
[b]Beijing Fine Ceramics Laboratory, State Key Laboratory of New Ceramics and Fine Processing, Institute of Nuclear and New Energy Technology, Tsinghua University, Beijing 100084, China

Received 27 June 2012; received in revised form 21 August 2012; accepted 23 August 2012
Available online 31 August 2012

Abstract

The strontium barium niobate (SBN) glasses were synthesized through a melt–quenching method. Crystallization mechanism for SBN glass–ceramics has been investigated by differential scanning calorimeter and optical microscope. The value of activation energy for the crystallization process indicates a controlling step of Si–O band breaking while optical microscope analysis shows a surface crystallization phenomenon. The effect of crystallization time on ac conductivities for glass and crystal phase was carried out by impedance analysis. The value of conductivity exhibits a rising trend as the crystallization time is increased. The results showed a better temperature–sensitive behavior for the crystal phase. In the conductivity spectra, Jonscher's universal power law and double power law were separately used to the glass and the crystal phase polarization effect. Results of dc conductivity versus measuring temperature from both effects well obey the Arrhenius law. Moreover, the value of the activation energy indicates an oxygen vacancy conductivity mechanism for the SBN glass–ceramics.

Keywords: Dielectric properties; Electrical conductivity; Glass–ceramics

1. Introduction

In recent years, great interest in finding ways to improve the energy storage properties for capacitors caused an attractive development in the dielectric materials. In order to reach a high energy density, characteristics such as high dielectric constant, high breakdown strength and low dielectric loss for materials are needed [1]. Among the dielectric materials available, ceramics have a high dielectric constant but a low breakdown strength, while polymers possess a large breakdown strength but a low dielectric constant. In contrast with the above two dielectrics, ferroelectric glass–ceramics with both a high dielectric constant and a large breakdown strength show a great potential in energy storage application [2–4].

Different types of ferroelectric glass–ceramics have been reported in literature. Since the pioneer work of Herczog [5], there have been many investigations on ferroelectric glass–ceramics containing major crystalline phases such as barium titanate with a perovskite structure. The key features of barium titanate family glass–ceramics are widely reported including phase evolution, crystallization kinetics, crystal morphology, and energy storage properties [3–7]. Nevertheless, as an important dielectric material with a structure similar to the perovskite one, glass–ceramics containing a major phase with a tungsten bronze structure have received less attention.

SBN ceramic is a typical material with the tungsten–bronze structure. It has been extensively used in modern electrooptic and photorefractive applications owing to its high electrooptic and piezoelectric coefficients [8]. In recent years, growing attention has been paid on its dielectric properties by varying its composition, heat–treatment conditions, etc [9,10]. A great potential for SBN to be an excellent dielectric material has been recognized. More and more reports for the composites based on the SBN ceramics appear. However, only a few attempts were found

*Corresponding author. Tel.: +86 10 80194055; fax: +86 10 89796022.
E-mail address: yzhang@tsinghua.edu.cn (Y. Zhang).

0272-8842/$ - see front matter © 2012 Elsevier Ltd and Techna Group S.r.l. All rights reserved.
http://dx.doi.org/10.1016/j.ceramint.2012.08.061

on SBN glass–ceramics. A study on the crystallization behavior and dielectric properties of SrO–BaO–Nb_2O_5–SiO_2 glasses was investigated by Shyu et al. [11,12]. Glass–ceramics containing SBN as a major phase was obtained. SBN content as well as the composite dielectric constant was found to be highly affected by the crystallization temperature. In the subsequent research [13], nucleating agents, such as BaF_2 were initially added to the glass system and yielded an improving crystallization behavior and good dielectric properties. In order to further understand the crystallization behavior of the SBN glass–ceramics and their resulting dielectric properties, further investigations were carried out in our lab. An interesting surface crystallization behavior was obviously observed as the crystallization time was changed. In this work, we will disclose the surface crystallization process by an optical microscope and discuss the crystallization mechanism with the measurement results of differential scanning calorimeter. Moreover, ac conductivity variation for different microelements contained in the SBN glass–ceramics was measured and interpreted as a function of the crystallization time.

2. Experimental procedure

2.1. Sample preparation

A glass with the composition 22.5 SrO, 22.5 BaO, 15 Nb_2O_5, and 40 SiO_2 (mol%) was prepared from reagent grade $SrCO_3$, $BaCO_3$, Nb_2O_5, and SiO_2. Well mixed powder containing appropriate ratios of the above chemicals was melted in a platinum crucible for 6 h at 1500 °C. Then the melted glass was poured into a copper cylinder mold, annealed at 600 °C for 12 h and furnace–cooled to room temperature.

The as–quenched glass was sectioned into disk–shaped samples of 0.8 mm in thickness by a diamond saw and then heat–treated with the heating rate of 5 °C/min at 950 °C for 0, 1, 3 and 5 h, respectively. To facilitate the following application, the glasses from the as–annealed samples along with the heat–treated ones were denoted as SBN–0, SBN–1, SBN–3 and SBN–5 respectively. Finally, silver paste was coated onto both surfaces of the specimens as electrodes and subsequently fired at 600 °C for 20 min for the following dielectric measurements.

2.2. Characterization

A differential scanning calorimeter (DSC) (NETZSCH STA 449C) was used to determine the glass transition temperature (T_g) and the crystallization temperatures (T_p). Approximately 0.5 g fine–ground glass powder was analyzed from room temperature to 1100 °C at the heating rates (5, 10, 15 and 20 °C/min). Cross–section morphology observation for the well–prepared glass–ceramics was performed by the field emission scanning electron microscopy (FE–SEM; Model Quanta 200 FEG, FEI, Netherlands) and the optical microscope (OM, CMM–33E). Crystal layer thickness was also measured from the microscopic observations and several measurements were made and averaged for each presented value. The room–temperature dielectric constant and dielectric loss were measured by means of a LCR meter (HP4284A Hewlett–Packard, Palo Alto, CA). Complex impedance spectroscopy over frequencies from 20 Hz to 1 MHz in a temperature range of 500 to 560 °C was measured using the same LCR meter with ac amplitude of 2.5 V.

3. Results and discussion

3.1. Crystallization mechanism

Fig. 1 (a) is the DSC curve for the glasses heat treated at different heating rates ranging from 5 to 20 °C/min. As is shown in each curve, there is only one exothermic peak for this system which should be attributed to the crystallization of the SBN phase. Increasing the heating rate, both the glass transition temperature (T_g) and the peak crystallization temperature (T_p) for the SrO–BaO–Nb_2O_5–SiO_2 system increased. The variation of T_p with the heating

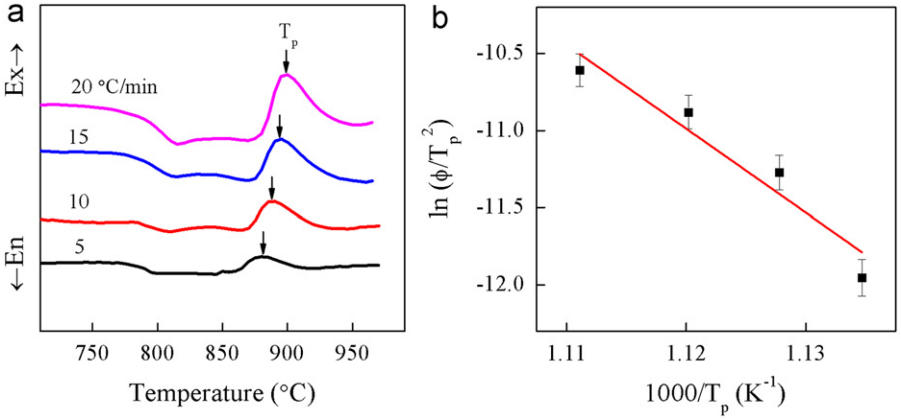

Fig. 1. (a) DSC curves of the annealed SrO–BaO–Nb_2O_5–SiO_2 glasses with different heating rates; (b) plots of $\ln(\phi/T_P^2)$ vs $1/T_p$ from which the crystallization activation energy is estimated.

rate follows the Kissinger equation [14]:

$$\ln\left(\phi/T_p^2\right) = -E/RT_P + \text{constant}. \quad (1)$$

Where T_p is the peak crystallization temperature, ϕ is the heating rate, R is the gas constant and E is the activation energy for crystallization.

Fitting $\ln\left(\phi/T_p^2\right)$ versus $1/T_p$ plot with the above equation, a straight line was obtained in Fig. 1 (b). The activation energy for the SBN crystallization process is calculated to be 462 kJ/mol from the slope ($-E/R$) of the line. For the phase transformation in glasses, two procedures, dissociation of ions and migration of dissociated ions, must be involved. Since the activation energy value is very close to the breaking energy of Si–O bonds (457 kJ/mol) [14], it is indicated that the mechanism of SBN crystal growth is mainly controlled by Si–O bonds broken in the atom rearrangement.

3.2. Optical microscope analysis

Figs. 2 and 3 are the cross–section morphology for the SBN glass–ceramics with different crystallization time, which was investigated by optical microscope. A predominant surface crystallization process is observed. As can be clearly seen from the pictures, crystals are inclined to initially precipitate at the sample surface for the SrO–BaO–Nb_2O_5–SiO_2 system. By considering the crystallization mechanisms in many other composite systems [15,16], this phenomenon may be caused by several factors, such as the rough surface morphology, different surface chemistries, and foreign impurities. All of these elements can lead a lower surface activation energy which can easily provide a nucleation site for crystallization. Samples without bulk crystallization can be imagined as a sandwich with a high resistive glass phase in the center. As the crystallization time is increased, the crystal layer will grow further to the interior area. The dense and homogenous layer with a white color marked in Figs. 2 and 3 represent the precipitation of SBN crystalline phase. And the thickness of crystallization layer for each sample was averaged by several measurements and plotted as a function of crystallization time, as shown in Fig. 4. Combined with Figs. 3 and 4, we can see that the crystalline layer thickness (L) gradually increases with the increase in crystallization time (t) and the layer growth approximately conforms to the parabolic law. For further increase in the crystallization time, bulk crystallization was observed. Also crystal morphology and size hardly change even after the crystallization time is increased to 5 h at 950 °C.

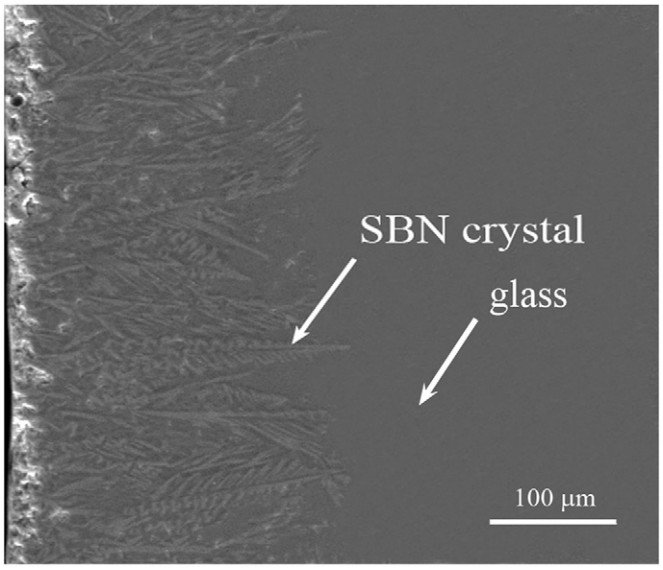

Fig. 2. SEM micrograph of the fracture surface for SBN–1.

3.3. Dielectric properties

Fig. 5 shows the variation of room–temperature dielectric constant and dielectric loss with the crystallization time measured at 1 kHz. As is shown in Fig. 5, the glass sample without crystallization exhibits a low dielectric constant (~10) indicating that there is hardly any crystal in the glass matrix. But extending the crystallization time, the value of dielectric constant begins to increase and finally achieves a nearly stable value (~460) after 5 h which is about 45 times higher than that of the SBN–0 sample. And the prominent enhancement in dielectric constant is primarily attributed to the crystallization of the SBN crystals with high dielectric constant [10]. In contrast, dielectric loss of all samples had small changes in value and fluctuated around 0.03. A slight increase of dielectric loss was observed for the samples with long crystallization time compared with the SBN–0 and SBN–1 samples.

3.4. AC conductivity

AC conductivity analysis is a useful method to distinguish in between different relaxation mechanisms and contributing factors to dielectric properties. It has been widely used in ionic oxides [17], glasses [18] and ceramic systems [19], etc. Different micro–elements such as grain, grain boundary and electrode with their dielectric/electrical contributions can be separated out through their frequency or temperature dependent response characteristics. In this work, impedance spectroscopy measurement for the SBN glass–ceramics with different crystallization time was carried out from 500 to 560 °C in the frequency range of 20 to 10^6 Hz. And then the electrical conductivity was calculated from the impedance data using the following equation:

$$\sigma(\omega) = LZ'/S\left(Z'^2 + Z''^2\right). \quad (2)$$

Where $\sigma(\omega)$ is the ac conductivity, Z' and Z'' are the real and imaginary parts of the impedance, L is the thickness and S is the electrode area coated on the surfaces of the samples.

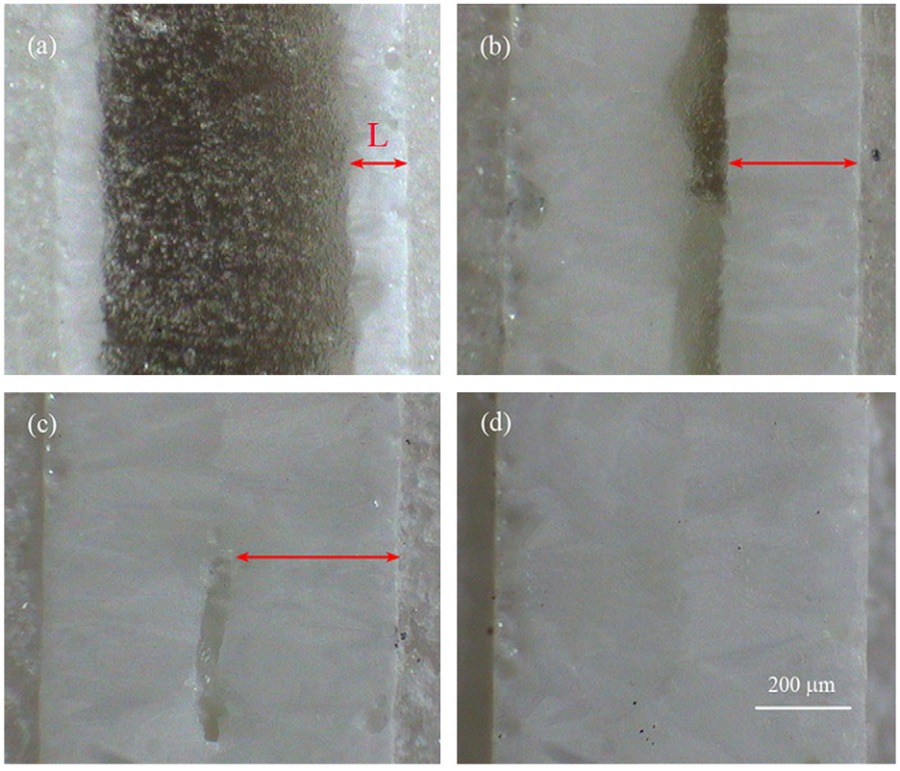

Fig. 3. Optical microscope photographs of the fracture morphology for SBN glass–ceramics with different crystallization time (a) SBN–0.5, (b) SBN–2, (c) SBN–3, and (d) SBN–5.

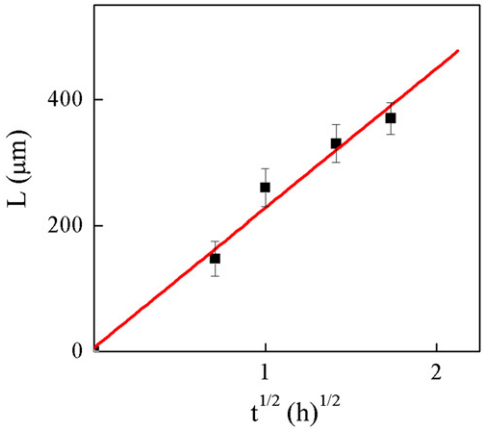

Fig. 4. Variation of the crystalline layer thickness (L) with the square root of crystallization time (t).

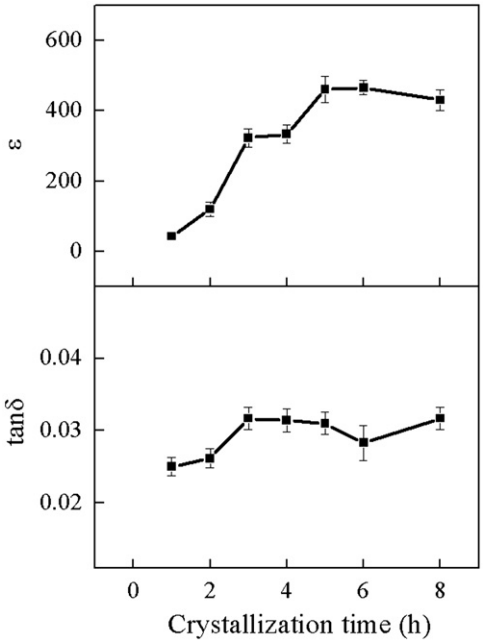

Fig. 5. Room–temperature dielectric constant and dielectric loss as a function of the crystallization time measured at 1 kHz.

Fig. 6 (a)–(d) show the obtained frequency–dependent ac conductivity at various temperatures for the four samples. As is shown, each curve in Fig. 6 is found to exhibit a similar variation tendency with frequency. In the low frequency regions, a nearly constant conductivity is observed, where charge transport can be explained by a hopping model [20]. According to this model, ions jump from one site to the adjacent vacancy successfully resulting in a long–range transitional motion of ions contributing to the dc conductivity. In contrast, in the high frequency region, a dispersive region attributed to ac conductivity is noteworthy, where the conductivity relaxation is mainly caused by the forward–backward hopping mechanism of the ions.

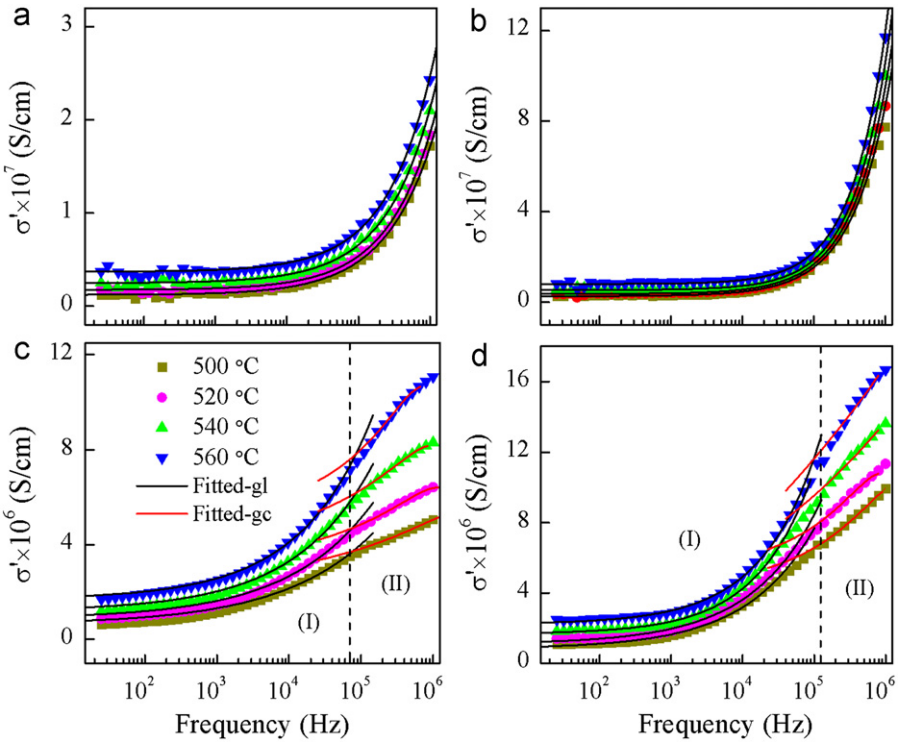

Fig. 6. Frequency–dependent ac conductivity at various temperatures for all the samples (a) SBN–0, (b) SBN–1, (c) SBN–3, and (d) SBN–5.

The samples with different crystallization time exhibit a different temperature–related conductivity behavior. As is illustrated in Fig. 6 (a) and (b), ac conductivity is insensitive to the measuring temperature in the whole frequency range. But when the crystallization time is increased, the ac conductivities of SBN–3 and SBN–5 samples are found to become strongly dependent on the temperature. This phenomenon indicates that the hopping process between two sites separated by an energy barrier is easier thermally activated in the SBN crystalline phase than in the glass matrix.

For SBN–0 and SBN–1 samples, the frequency–related conductivity data can be well fitted by Johnscher's universal power law in the measuring temperature range:

$$\sigma' = \sigma_{dc} + Af^n. \tag{3}$$

Where σ' is the real conductivity, σ_{dc} is dc conductivity and parameters A, n $(0<n<1)$ are temperature and material intrinsic property dependent constants [20].

But for SBN–3 and SBN–5 samples, no accurate fit to the conductivity data using Eq. (3) can be obtained in the investigated temperature range. According to our previous research, bulk crystallization had already been observed for the SBN–3 and SBN–5 samples. Two different relaxation responses were observed in impedance spectrum originating from the glass matrix and the SBN crystalline phase, respectively. Looking at the ac conductivity curves in Fig. 6 (c) and (d) carefully, some anomalies could be observed in the frequency–dependent regions suggesting the existence of multiple relaxation processes. As is reported in the literature, the ac conductivity–spectrum consisting of two relaxation contributions should be divided into two parts with different models to describe the conductivity behavior [20,21]. Based on this method, frequency–dependent conductivity in Fig. 6 (c) and (d) are separated into two parts: data in part I obey the Johnscher's universal power law well while part II can be described with a double power law as follows [20,21]:

$$\sigma' = \sigma_b + A_1 f^n + A_2 f^s. \tag{4}$$

Where σ_b is the crystal dc conductivity, A_1, A_2, n $(0<n<1)$ and s $(0<s<1)$ are four temperature and material intrinsic property dependent constants. $\sigma_b + A_1 f^n$ characterizes the contributions from the crystalline phases and $A_2 f^s$ is corresponding to a transition between the glass matrix and crystalline phase relaxations.

From the power law analysis with Eqs. (3) and (4), the fitting results are shown in Fig. 6. As can be seen from Fig. 6, the experimental data were perfectly fitted by solid lines. Parameters for the glass and crystal phases obtained from the fitting line are listed in Tables 1 and 2, respectively. In the measuring temperature range, n takes on a major trend of diminution before and after bulk crystallization while s increases slightly as the crystallization time is increased. As the exponent in the above equations represents the degree of interaction between mobile ions and the environment surrounding them [22], the crystallization time dependent variation of n and s

Table 1
Parameters for the glass phase obtained from the fitting line with Johnscher's universal power law.

		500 °C	520 °C	540 °C	560 °C
SBN-0	$\sigma_{dc} \times 10^8$ (S/cm)	1.21	1.76	2.49	3.70
	$A \times 10^{10}$	0.22	0.17	0.21	0.19
	n	0.64	0.67	0.66	0.67
SBN-1	$\sigma_{dc} \times 10^8$ (S/cm)	2.65	3.67	5.36	7.98
	$A \times 10^{10}$	0.10	0.08	0.06	0.05
	n	0.82	0.84	0.87	0.89
SBN-3	$\sigma_{dc} \times 10^8$ (S/cm)	63.5	87.6	121	170
	$A \times 10^{10}$	625	576	508	433
	n	0.35	0.37	0.40	0.44
SBN-5	$\sigma_{dc} \times 10^8$ (S/cm)	83.7	111	168	224
	$A \times 10^{10}$	335	350	148	177
	n	0.46	0.46	0.56	0.55

Table 2
Parameters for the crystalline phase obtained from the fitting line with double power law.

		500 °C	520 °C	540 °C	560 °C
SBN-3	$\sigma_{dc} \times 10^8$ (S/cm)	211	304	376	514
	$A \times 10^{10}$	1050	440	635	159
	n	0.24	0.32	0.32	0.45
SBN-5	$\sigma_{dc} \times 10^8$ (S/cm)	339	463	606	721
	$A \times 10^{10}$	202	116	21	0.17
	n	0.38	0.42	0.49	0.54

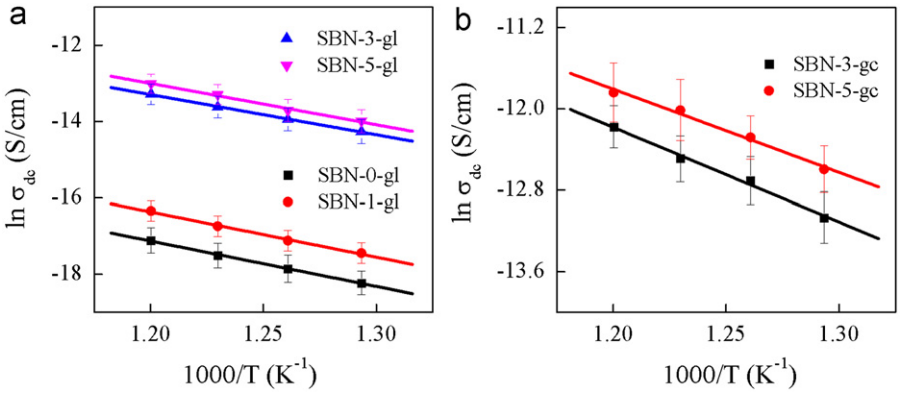

Fig. 7. Variation of $\ln\sigma_{dc}$ with the inverse of absolute temperature ($10^3/T$) for all the SBN glass–ceramics with different crystallization time (a) glass phase; (b) crystalline phase.

indicates a weaker and stronger interaction of ions for glass and crystalline phases respectively. Besides, there is an increase for the σ_{dc} value with the rise of the measuring temperature for all samples. An order of magnitude enhancement in conductivity is observed as the crystallization time was prolonged to 3 h. From Figs. 2 and 3, we already know that the crystals initially precipitate at the surface area and gradually grow to the interior. For SBN–0 and SBN–1, the crystalline phase is distributed in the glass matrix so isolatedly that the charge carriers have to pass through the high resistive glass phase for transfer, which leads to a relatively low conductivity. But when the bulk crystallization happened, the connectivity between the crystalline phases is realized which creates an easier pass way for charge carriers resulting in higher conductivity.

The temperature–dependent σ_{dc} values for the glass and crystalline phases of all specimens exhibit good linearities in Fig. 7 (a) and (b) which follow the Arrhenius relations:

$$\sigma_{dc} = \sigma_0 \exp\left(-E_a/k_B T\right). \quad (5)$$

Where σ_0 is a constant, E_a is the activation energy, k_B is the Boltzmann constant and T is the absolute temperature.

Via the slope of the fitted straight lines, the activation energy values were calculated out and listed in Table 3. As can be seen from Table 3, the activation energy value for the crystalline phase is smaller than that of the glass phase

Table 3
Activation energy calculated from the dc conductivity for the SBN glass–ceramics with different crystallization time (E_{gl}, E_{gc} represent the activation energy for the glass and the crystalline phase respectively).

	SBN-0	SBN-1	SBN-3	SBN-5
E_{gl} (eV)	1.03	1.02	0.91	0.93
E_{gc} (eV)	–	–	0.85	0.79

indicating a better conductive property for the SBN phase. The activation energy for the glass phase (E_{gl}) is around 1.0 eV which is attributed to the diffusion of oxygen vacancies in the samples. With the rise of crystallization time, atom rearrangement during the crystallization process causes a change in the glass network leading to a slight decrease in E_{gl}. In opposite, a negligible change for the E_{gc} value implying that there is no change in the conduction mechanism for the crystalline phase after bulk crystallization.

4. Conclusions

The crystallization mechanism of the SBN glass–ceramics was investigated by the DSC method with different heating rates. The value of activation energy (462 kJ/mol) related to the crystallization process indicates a controlling step of Si–O bond breaking. Optical observation on the cross–section of the samples shows an obvious surface crystallization phenomenon for the SBN glass–ceramics. The crystal layer thickness gradually increased with the rise of crystallization time and the layer growth approximately conforms to the parabolic law before bulk crystallization sets in. A prominent enhancement for the room–temperature dielectric constant with the crystallization time is primarily attributed to the precipitation of SBN crystals with high dielectric constant. AC conductivity analysis was employed to separate the conduction behaviors originating from different micro–elements of the SBN glass–ceramics. The conductivity results show a temperature–sensitive behavior for the crystalline phase in the high frequency region, which indicates that the hopping process in the SBN crystalline phase is easier thermally activated than in the glass matrix. Two models, Jonscher's universal power law and the double power law, are respectively employed to fit the experimental conductivity data for the glass matrix and crystalline phase with a good fitting result. As the crystallization time is prolonged, both the dc and ac conductivities show a rising trend. The exponent in the power law equations related to the glass phase exhibits a decrease while an increase in the amount of crystalline phase is observed. The activation energy values indicate an oxygen vacancy conductivity mechanism at the investigated temperature range for the SBN glass–ceramics.

Acknowledgments

The authors wish to thank the National Natural Science Foundation of China (Grant no. 50977049,51072016) and State Key Laboratory of New Ceramic and Fine Processing (Tsinghua University KF1014) for financial support and Drs. J. Wang, B.H. Wen, S. Wang, Q. Zhang for valuable discussions.

References

[1] M.J. Pan, C.A. Randall, A brief introduction to ceramic capacitors, IEEE Electrical Insulation Magazine 26 (2010) 44–50.
[2] C.T. Cheng, M. Lanagan, B. Jones, J.T. Lin, M.J. Pan, Crystallization kinetics and phase development of PbO–BaO–SrO–Nb_2O_5–B_2O_3–SiO_2–based glass–ceramics, Journal of the American Ceramic Society 88 (2005) 3037–3042.
[3] E.P. Gorzkowski, M.J. Pan, B. Bender, C.C.M. Wu, Glass–ceramics of barium strontium titanate for high energy density capacitors, Journal of Electroceramics 18 (2007) 269–276.
[4] E.P. Gorzkowski, M.J. Pan, B. Bender, C.C.M. Wu, Effect of additives on the crystallization kinetics of barium strontium titanate glass–ceramics, Journal of the American Ceramic Society 91 (2008) 1065–1069.
[5] A. Herczog, Microcrystalline $BaTiO_3$ by crystallization from glass, Journal of the American Ceramic Society 47 (1964) 107–115.
[6] K. Yao, L.Y. Zhang, X. Yao, Preparation and properties of barium titanate glass–ceramics sintered from sol–gel derived powders, Journal of Materials Science 32 (1997) 3659–3665.
[7] J.C. Chen, Y. Zhang, C.S. Deng, X.M. Dai, Improvement in the microstructures and dielectric properties of barium strontium titanate glass–ceramics by AlF_3/MnO_2 addition, Journal of the American Ceramic Society 92 (2009) 1863–1866.
[8] Y.Q. Qu, A.D. Li, Q.Y. Shao, Y.F. Tang, D. Wu, C.L. Mak, Structure and electrical properties of strontium barium niobate ceramics, Materials Research Bulletin 37 (2002) 503–513.
[9] P.K. Patro, R. Khatirkar, I. Samajdar, A.R. Kulkarni, C.S. Harendranath, Strontium barium niobate–relating structral developments and dielectric constant, Journal of the European Ceramic Society 27 (2007) 2255–2263.
[10] M.S. Kim, J.H. Lee, J.J. Kim, H.Y. Lee, S.H. Cho, Microstructure and dielectric characteristics of tungsten bronze structured SBN70 ceramics: effect of Nb_2O_5 content, Journal of the European Ceramic Society 22 (2002) 2107–2113.
[11] J.J. Shyu, C.H. Chen, Sinterable ferroelectric glass–ceramics containing (Sr, Ba)Nb_2O_6 crystals, Ceramics International 29 (2003) 447–453.
[12] J.J. Shyu, J.R. Wang, Crystallization and dielectric properties of SrO–BaO–Nb_2O_5–SiO_2 tungsten bronze glass–ceramics, Journal of the American Ceramic Society 83 (2000) 3135–3140.
[13] Y.K. Zeng, X.Y. Qin, S.L. Jiang, G.Z. Zhang, L. Zhang, Effect of BaF_2 addition on crystallization kinetics and dielectric properties of B_2O_3–Nb_2O_5–SrO–BaO glass–ceramics, Journal of the American Ceramic Society 94 (2011) 469–473.
[14] J.C. Chen, Y. Zhang, C.S. Deng, X.M. Dai, Crystallization kinetics and dielectric properties of barium strontium titanate based glass–ceramics, Materials Chemistry and Physics 121 (2010) 109–113.
[15] Y. Diao, A.S. Myerson, T.A. Hatton, B.L. Trout, Surface design for controlled crystallization: the role of surface chemistry and nanoscale pores in heterogeneous nucleation, Langmuir: The ACS Journal of Surfaces and Colloids 27 (2011) 5324–5334.
[16] E.D. Zanotto, Experimental studies of surface nucleation and crystallization of glasses, Ceramic Transactions 30 (1993) 65–74.
[17] D.P. Almond, A.R. West, Anomalous conductivity prefactors in fast ions conductors, Nature 306 (1983) 456–457.
[18] P. Muralidharan, N. Nallamuthu, I. Prakash, N. Satyanarayana, M. Venkateswarlu, AC conductivity and electrical modulus studies on lithium vanadophosphate glasses, Journal of the American Ceramic Society 90 (2007) 125–131.

[19] S. Selvasekarapandian, M. Vijayakumar, The ac impedance spectroscopy studies on $LiDyO_2$, Materials Chemistry and Physics 80 (2003) 29–33.
[20] W. Chen, W. Zhu, O.K. Tan, X.F. Chen, Frequency and temperature dependent impedance spectroscopy of cobalt ferrite composite thick films, Journal of Applied Physics 108 (2010) 034101.
[21] L. Zhang, Electrode and grain–boundary effects on the conductivity of $CaCu_3Ti_4O_{12}$, Applied Physics Letters 87 (2005) 022907.
[22] R.H. Chen, R.Y. Chang, S.C. Shern, Dielectric and ac ionic conductivity investigations in $K_3H(SeO_4)_2$ single crystal, The Journal of Physics and Chemistry of Solids 63 (2002) 2069–2077.